

LCLA: Language-Conditioned Latent Alignment for Vision-Language Navigation

Nitesh Subedi*, Adam Haroon*, Samuel Tetteh*, Prajwal Koirala†, Cody Fleming*, and Soumik Sarkar*

*Iowa State University

Ames, Iowa 50014, USA

Emails: (nitesh, aharoon, samtett, flemingc, soumiks)@iastate.edu

†Cornell University

Ithaca, New York 14850, USA

Email: pk596@cornell.edu

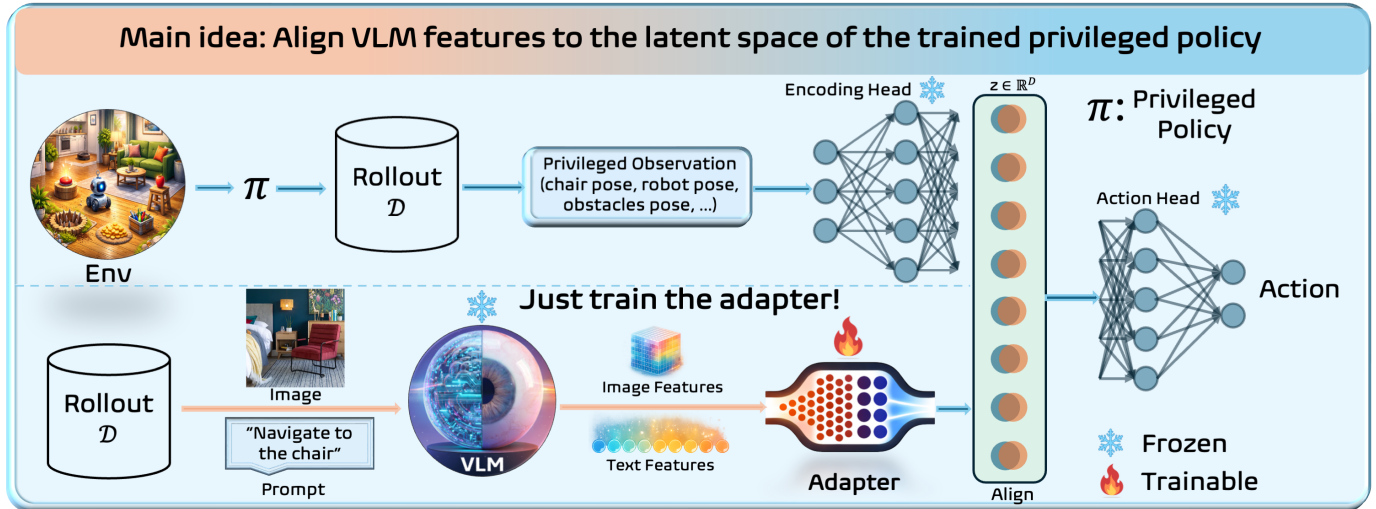


Fig. 1: Overview of latent representation alignment with a frozen privileged policy. An expert policy π is first trained using privileged state observations (e.g., object poses, robot pose, and environment geometry) and induces a task-relevant latent representation $z \in \mathbb{R}^D$ sufficient for control. Rollouts collected from this policy provide supervision for learning a lightweight adapter on top of a pre-trained vision-language model (VLM). The adapter aligns image and text embeddings to the expert’s latent space, while the expert policy and action head remain frozen. At deployment, actions are produced by mapping visual and language inputs through the VLM and adapter into the expert-defined latent space and reusing the frozen action head.

Abstract—We propose LCLA (Language-Conditioned Latent Alignment), a framework for vision-language navigation that learns modular perception–action interfaces by aligning sensory observations to a latent representation of an expert policy. The expert is first trained with privileged state information, inducing a latent space sufficient for control, after which its latent interface and action head are frozen. A lightweight adapter is then trained to map raw visual–language observations, via a frozen vision–language model, into the expert’s latent space, reducing the problem of visuomotor learning to supervised latent alignment rather than end-to-end policy optimization. This decoupling enforces a stable contract between perception and control, enabling expert behavior to be reused across sensing modalities and environmental variations. We instantiate LCLA and evaluate it on a vision-language indoor navigation task, where aligned latent spaces yield strong in-distribution performance and robust zero-shot generalization to unseen environments, lighting conditions, and viewpoints while remaining lightweight at inference time.

I. INTRODUCTION

A central challenge in embodied artificial intelligence is learning representations that support reliable decision making from high-dimensional sensory inputs [21, 20]. Navigation provides a canonical instance of this problem: while control depends on low-dimensional geometric quantities such as goal direction and obstacle proximity, agents deployed in realistic settings must infer these variables from raw RGB observations and natural-language instructions. When compact state representations are available, classical planning and policy-gradient methods perform well [34, 17]; however, bridging the gap between perception and control from raw sensory inputs remains challenging [32, 9].

Vision–language navigation (VLN) further amplifies this difficulty [3, 16, 15, 22, 14, 2, 42]. Visual uncertainty due to viewpoint changes, lighting variation, and clutter is

compounded by linguistic ambiguity, as instructions may be relational or underspecified. Consequently, VLN becomes fundamentally a representation learning problem rather than a pure control problem.

A common approach is to train policies end-to-end from pixels and language to actions [26, 43, 33]. While effective in simulation, such methods often exhibit poor generalization and high sample complexity, as learned representations exploit environment-specific correlations rather than recover task-relevant structure [1, 9]. This brittleness stems from a representation mismatch: control policies require compact, egocentric abstractions, whereas sensory observations are high-dimensional and entangled.

We introduce **Language-Conditioned Latent Alignment (LCLA)**, a framework that explicitly decouples perception from control by reframing navigation as a representation alignment problem. We first train a privileged expert policy using concise geometric state information and then freeze its latent interface and action head. Perception is addressed separately by training a vision–language adapter to map RGB observations and language instructions into the expert’s latent space, using fully supervised latent alignment rather than action imitation. This design leverages frozen vision–language models [30, 39] for rich visual and semantic features while isolating representation learning from control optimization.

LCLA builds on prior work using privileged information and teacher–student supervision [6, 23, 28], but differs in a key respect: instead of distilling behavior at the action level or jointly learning representations and control, we align perception to a fixed, task-centric latent state of a frozen expert. This latent provides dense, unambiguous supervision and enables the expert controller to be reused across sensing modalities and environments without retraining control.

We instantiate LCLA as a *Language-Conditioned Latent Alignment Adapter (LCLAA)* for indoor object navigation. Despite training in a single environment with limited object diversity, the resulting agent generalizes zero-shot to unseen scenes and objects, demonstrating that recovering the *right representation* is sufficient for robust navigation under limited supervision.

Our contributions are:

- **Latent Decoupling of Perception and Control:** A framework that solves navigation in a frozen, task-centric latent space defined by a privileged expert.
- **Vision–Language Latent Alignment:** A supervised formulation that maps vision–language embeddings to an expert’s internal navigation state, avoiding direct action imitation.
- **Modular Grounding of Frozen VLMs:** A lightweight adapter-based approach that enables reuse of expert policies across perception backbones and modalities.

We ablate LCLA along two axes: replacing latent alignment with direct action prediction (Language-Conditioned Behavior Cloning, LCBC), and removing explicit language conditioning by aligning pooled vision–language embeddings (PELA). In both cases, LCLA outperforms the ablated variants by a

substantial margin, demonstrating that neither end-to-end imitation nor latent alignment alone is sufficient. By disentangling what to do from how to see, LCLA reframes navigation as a problem of representation alignment rather than end-to-end policy learning.

II. RELATED WORK

A. Visual Navigation from Raw Observations

Visual navigation has long been studied as learning control from high-dimensional sensory inputs. Early end-to-end visuomotor approaches map pixels directly to actions using reinforcement learning [26, 43, 33], but often generalize poorly under appearance or layout changes. Cognitive mapping and planning-based methods learn latent spatial representations to support long-horizon reasoning [10, 5], yet remain vulnerable to perceptual aliasing and shortcut learning [9].

B. Privileged Information and Asymmetric Learning

Privileged learning frameworks stabilize training by exposing experts or critics to full state information [29, 31]. Learning by Cheating [6] and related methods distill privileged expertise into deployable visual policies via imitation. Similar ideas have been applied to crowd navigation [27] and agile locomotion [4]. However, action imitation can be ambiguous when multiple behaviors are valid. Teacher–student distillation frameworks such as CaT and SITT [41, 25] similarly leverage expert supervision but typically distill actions or values rather than internal representations. In contrast, we align directly to the expert’s latent state, enabling reuse of frozen control policies.

C. Representation Learning for Control

Representation learning aims to improve robustness and sample efficiency in reinforcement learning. Self-supervised objectives [35, 19] and data augmentation [38] improve generalization from pixels, while model-based methods learn compact latent dynamics for planning [11, 12]. Bisimulation-based approaches explicitly target task-relevant abstractions [40]. However, these representations are typically learned jointly with the policy and remain tightly coupled to the observation modality and training environment.

D. Vision–Language Navigation

VLN conditions navigation on natural-language instructions, introducing grounding and ambiguity challenges [3, 8, 18]. Large VLMs such as CLIP and SigLIP-2 [30, 37] enable zero-shot and language-conditioned navigation [7, 24, 36]. Map-centric methods integrate VLM features into spatial representations for querying and planning [15]. Recent work explores efficient training and adaptation in continuous environments [2, 42, 14, 16]. Most approaches, however, treat VLM features as generic perceptual inputs and train downstream policies end-to-end, leaving alignment to task-optimal control representations implicit.

E. Latent Interfaces Between Perception and Control

Several works advocate structured latent spaces as interfaces between perception and decision making [11, 12, 5]. Unlike methods that learn latents jointly with perception and control, our approach aligns vision–language observations to a *predefined* latent space induced by a privileged expert policy, enabling modular reuse of control and grounding of frozen foundation models into task-centric representations.

III. METHODOLOGY

A. Overview: Action–Perception Decoupling

Our approach explicitly decouples perception from control, as illustrated in Fig. 1. Instead of learning a monolithic policy that maps pixels and language directly to actions, we decompose the agent into two modules with clearly separated roles: (i) a *privileged expert policy* that performs action selection in an abstract, control-centric latent space, and (ii) a *visual-linguistic adapter* that maps raw sensory observations into this latent space.

The privileged expert can be viewed as a *frozen brain*: it is trained once using compact, privileged state information and then kept fixed. The adapter acts as a *learned eye*: it is the only trainable component exposed to images and language, and its sole objective is to translate perceptual inputs into the expert’s internal representation. This design enforces a stable interface between perception and control and isolates generalization entirely to the adapter.

Formally, the expert policy is denoted $\pi_{\text{priv}}(a | s)$, where s_t is a privileged state and a_t is an action (e.g., a continuous velocity command). We decompose the expert into an encoding head π_{priv}^e and an action head π_{priv}^a :

$$z_t = \pi_{\text{priv}}^e(s_t), \quad a_t = \pi_{\text{priv}}^a(z_t),$$

where z_t is a latent representation sufficient for decision making. The adapter f_θ takes an RGB image I_t and a language instruction L and predicts a latent \hat{z}_t in the same space:

$$\hat{z}_t = f_\theta(I_t, L).$$

Adapter training enforces $\hat{z}_t \approx z_t$, aligning perceptual representations with the expert’s internal state. At inference time, action selection proceeds by chaining frozen modules:

$$I_t, L \xrightarrow{f_\theta} \hat{z}_t \xrightarrow{\pi_{\text{priv}}^a} a_t.$$

B. Stage 1: Privileged Expert Policy

In Stage 1, we train the privileged expert policy π_{priv} in an idealized setting where the agent has access to compact, low-dimensional state variables such as goal direction, distances to obstacles, and relative pose information. These states are by construction invariant to visual appearance, lighting, and texture.

The expert is trained using standard reinforcement learning to reliably solve navigation tasks. Because its decisions are expressed purely in terms of abstract geometric quantities, the learned policy captures task-invariant control logic (e.g.,

obstacle avoidance, goal-directed motion) independent of sensory modality. After training, both the encoder π_{priv}^e and the action head π_{priv}^a are frozen and never updated again. We do not assume that the expert latent z_t is disentangled or semantically interpretable. Instead, we treat it as a *functional control interface*: a representation that is sufficient and stable for action selection. Our objective is not to recover human-interpretable factors, but to align perception to an internal representation that the expert policy already uses effectively for navigation. The latent dimensionality ablation in Sec. V further shows that not all intermediate representations are equally suitable for this role.

C. Stage 2: Visual–Linguistic Adapter

Stage 2 trains the adapter f_θ to map raw observations into the expert’s latent space. This stage is formulated as a supervised learning problem. We generate training data by rolling out the frozen expert in the environment while simultaneously rendering visual observations. At each time step, we record tuples (s_t, I_t, L) and compute the corresponding expert latent $z_t = \pi_{\text{priv}}^e(s_t)$.

The adapter is trained to predict \hat{z}_t from (I_t, L) by minimizing an alignment loss between \hat{z}_t and z_t . No reinforcement learning is performed at this stage, and the expert policy remains unchanged throughout.

a) Visual Backbone: To extract perceptual features, we employ a pre-trained vision–language model (VLM) as a frozen backbone. Given an image I_t , the VLM’s vision transformer produces patch-level visual embeddings V_t , while the text encoder maps the instruction L to a text embedding T . Both encoders are frozen to preserve their broad semantic priors and to limit learning to the adapter.

b) Adapter Architecture: The adapter implements a lightweight, trainable mapping

$$f_\theta : (V_t, T) \rightarrow \hat{z}_t,$$

and may be instantiated using attention-based or transformer-style architectures. In our implementation (Fig. 2), the adapter uses language-conditioned attention to select task-relevant visual information before producing the aligned latent. The adapter serves as a translator between the VLM’s representational space and the expert’s control-centric latent space.

Our language evaluation focuses on controlled, templated instructions with relational structure in order to isolate perceptual grounding effects. Evaluating free-form, naturalistic instructions and more complex linguistic phenomena is an important direction for future work, but is orthogonal to our core question of whether expert latents can be reliably recovered from vision–language inputs.

D. Inference

At deployment, the agent operates without access to privileged state. At each time step, it observes an RGB image I_t and instruction L , extracts frozen visual and language embeddings (V_t, T) , predicts $\hat{z}_t = f_\theta(V_t, T)$, and executes the action

$$a_t = \pi_{\text{priv}}^a(\hat{z}_t).$$

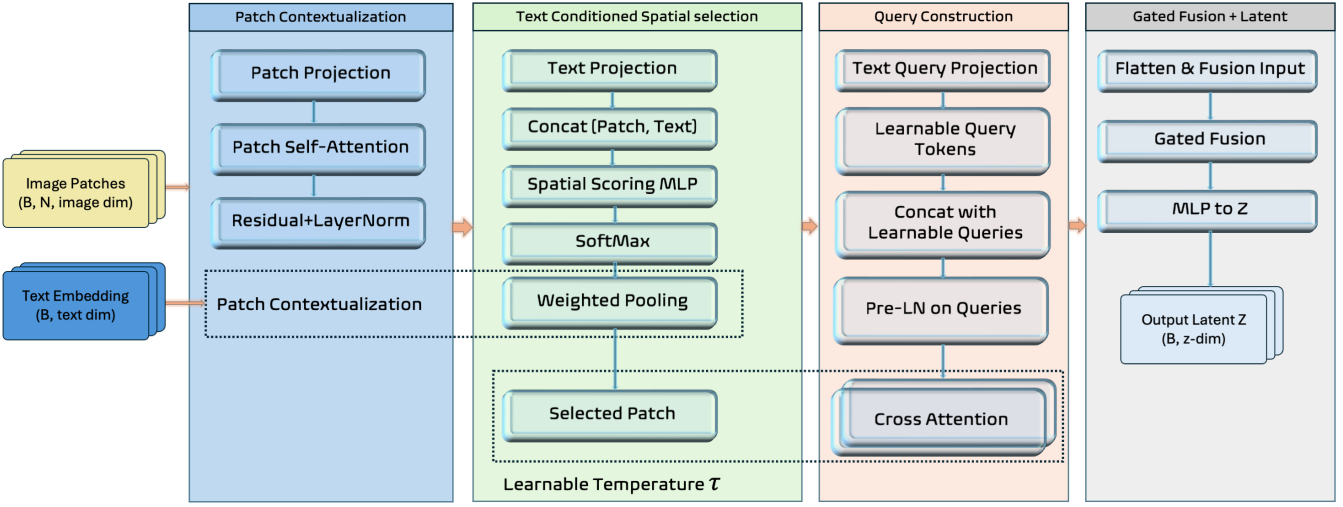


Fig. 2: **Architecture of the Language Conditioned Latent Alignment Adapter (LCLAA).** The model takes image patches and a text embedding as input. (1) Patches are first contextualized via self-attention. (2) A spatial bottleneck then uses text-conditioned importance scores to select relevant visual context (soft selection). (3) A query generation module combines the text embedding with learnable queries. (4) These queries attend to the selected visual context through stacked cross-attention blocks. (5) Finally, a gated fusion mechanism combines the processed queries with the original text residual to produce the aligned latent representation Z

E. Key Property

Because the expert policy never observes pixels and the VLM is never optimized for control, the adapter is the *only* learned bridge between perception and action. This structural bottleneck enforces modularity, stabilizes control behavior, and enables systematic analysis of how perceptual errors propagate to actions, which we later quantify via latent-to-action sensitivity measures.

IV. CONTROLLED VALIDATION STUDY

We now validate the proposed *adapter-based latent alignment* framework (LCLA) introduced in Section III by instantiating a specific adapter architecture that we term **LCLAA** (Language Conditioned Latent Alignment Adapter). While our core method is architecture-agnostic (any adapter that maps frozen VLM embeddings to the privileged expert latent is compatible), we introduce LCLAA as a concrete realization to our method. We emphasize that LCLAA is used only for validation; the underlying principle is the latent alignment interface between a frozen VLM and a frozen privileged policy. Our evaluation is intentionally constrained to isolate representation alignment effects under controlled conditions. We do not aim to establish broad simulator-level generalization, but rather to test whether a frozen expert latent can be reliably recovered from vision-language inputs.

A. LCLAA: Language-Conditioned Latent Alignment Adapter

A central challenge in visuomotor navigation under distribution shift is preventing policies from exploiting spurious visual correlations that are predictive in training but irrelevant to task execution. When visual representations are directly pooled or flattened, background textures, lighting conditions,

and clutter can dominate learned features, resulting in brittle generalization. This issue is exacerbated when policies are trained end-to-end or via imitation without explicit structural constraints on perception.

Within the **LCLA** framework, LCLAA instantiates a perception module that aligns raw sensory observations to a task-centric latent representation learned by a privileged expert. LCLAA introduces an explicit *language-conditioned bottleneck* between perception and control, enforcing structural constraints that restrict information flow to instruction-relevant visual evidence while remaining compatible with a frozen expert.

At timestep t , the agent receives an RGB observation I_t and a natural language instruction L . A frozen vision–language model encodes these inputs as

$$V_t = \phi_{\text{img}}(I_t) \in \mathbb{R}^{N \times D_{\text{img}}}, \quad (1)$$

$$T = \phi_{\text{txt}}(L) \in \mathbb{R}^{D_{\text{txt}}}, \quad (2)$$

where $V_t = \{v_{t,i}\}_{i=1}^N$ denotes patch-level visual embeddings and T is a global text embedding. We just take the output of the last hidden state to get the patch level visual embeddings. The adapter maps (V_t, T) to a predicted expert-compatible latent $\hat{z}_t \in \mathbb{R}^{d_z}$,

$$\hat{z}_t = f_{\theta}(V_t, T), \quad a_t \sim \pi_{\text{priv}}(\hat{z}_t), \quad (3)$$

where π_{priv} is a frozen privileged policy trained on full state information.

a) Choice of expert latent interface: The privileged PPO policy is an Multi Layer Perceptron (MLP) of the form $\text{obs} \rightarrow 512 \rightarrow 256 \rightarrow 128 \rightarrow \text{action}$. We treat intermediate hidden activations as candidate expert latents. Concretely, for a chosen interface dimension $d_z \in \{512, 256, 128\}$, the

teacher latent $z_t^{(d_z)}$ is the PPO hidden activation at that layer. The corresponding downstream sub-network (the PPO layers mapping $z_t^{(d_z)}$ to actions) is frozen and used as the action head during deployment. We train a separate adapter for each d_z to predict $\hat{z}_t^{(d_z)}$ from frozen VLM features, and feed $\hat{z}_t^{(d_z)}$ into the matching frozen PPO suffix. This avoids any dimensionality mismatch and introduces no additional projection layers.

b) Language-Conditioned Visual Bottleneck: Patch embeddings are first contextualized using self-attention to incorporate spatial dependencies:

$$X_t = \text{MHSA}(V_t). \quad (4)$$

To identify instruction-relevant regions, LCLAA computes language-conditioned relevance scores

$$s_{t,i} = g_\theta([x_{t,i}; T]), \quad (5)$$

which are normalized to produce a distribution over patches,

$$\alpha_{t,i} = \frac{\exp(s_{t,i}/\tau)}{\sum_{j=1}^N \exp(s_{t,j}/\tau)}. \quad (6)$$

These weights define a differentiable bottleneck via a convex aggregation:

$$\bar{x}_t = \sum_{i=1}^N \alpha_{t,i} x_{t,i}. \quad (7)$$

This bottleneck ensures that downstream control has access only to a compact, instruction-conditioned summary of the visual scene.

c) Query-Based Refinement and Latent Projection.: To refine the bottleneck representation, LCLAA constructs a small set of queries consisting of a text-derived query and M learnable query tokens. These queries attend to the bottleneck representation via stacked cross-attention blocks:

$$Q_t^{(b+1)} = \text{CAB}_\theta(Q_t^{(b)}, \bar{x}_t), \quad b = 0, \dots, B-1. \quad (8)$$

where CAB=Cross Attention Blocks. The refined queries are fused with the text embedding through a learned gating mechanism and projected into the expert latent space:

$$\hat{z}_t = \text{MLP}_\theta \left(\text{Fuse}(Q_t^{(B)}, T) \right). \quad (9)$$

d) Training Objective.: Let z_t denote the latent representation produced by the privileged expert encoder. LCLAA is trained using a supervised latent alignment objective:

$$\mathcal{L} = \lambda_1 \mathcal{L}_{\text{contrast}} + (1 - \lambda_1) \|\hat{z}_t - z_t\|_2^2 + \lambda_2 \|\pi_{\text{priv}}^a(\hat{z}_t) - \pi_{\text{priv}}^a(z_t)\|_2^2, \quad (10)$$

where $\mathcal{L}_{\text{contrast}}$ encourages discriminative alignment in latent space and $\pi_{\text{priv}}^a(\cdot)$ denotes the action of the frozen expert policy. In our work, we have used both $\lambda_1=0.8$ and $\lambda_2=1$. Only the adapter parameters θ are optimized; both the vision-language encoder and expert policy remain fixed.

	Room A	Room B
Number of target objects	18	12
Seen object categories	Yes	Partial(2)
Novel object categories	No	Yes
Layout seen in training	Yes	No
Evaluation mode	Training / ID	Zero-shot OOD

TABLE I: Key differences between training and evaluation environments.

e) Design Rationale: The architectural components of LCLAA impose inductive biases that promote robust latent alignment rather than maximize task-specific capacity. Language-conditioned visual selection suppresses spurious correlations, the enforced bottleneck constrains perception to task-relevant evidence, and query-based cross-attention enables stable aggregation under varying scene complexity. Our objective is not to optimize a particular adapter architecture, but to demonstrate latent alignment as a viable and interpretable representation learning paradigm. Additional architectural details and robustness analyses are provided in the appendix.

B. Experimental Setup

a) Task: We evaluate on an object-goal navigation task. At the start of each episode, the agent is placed at a random pose in an indoor environment and receives a language instruction L specifying a target object category (e.g., “Navigate to the chair”). The episode succeeds if the agent reaches within a fixed radius of any instance of the target object, facing the goal to certain threshold, within a time limit. Additionally, for each goal, we train with 8 different prompts. Each prompts are different in the sense that some give relation with other objects in scene while some give color attribute. See figure 3.

b) Simulators and Environments: Our primary training and evaluation environment is built in a photorealistic simulator, Isaac Sim. We design two environment splits to measure in-distribution (Room A) performance and out-of-distribution (OOD) generalization (Room B). Room A serves as the training environment and contains 18 navigable target objects spanning common household categories (e.g., chair, table, cabinet). Object instances, layouts, and visual appearance in Room A are fully observed during training. Room B is held out entirely during training and is used exclusively for evaluation. It contains 12 target objects, including both category-overlapping instances with novel visual appearance and previously unseen object categories. In addition to object novelty, Room B differs in spatial layout, object arrangement, textures, and lighting conditions. This setting evaluates an agent’s ability to generalize beyond memorized visual cues to unseen environments with increased semantic and geometric diversity.

Importantly, no fine-tuning or adaptation is performed in Room B; all policies and adapters are evaluated zero-shot. While Room A and Room B share high-level task semantics, successful navigation in Room B requires robust perception



Prompt Template Families (Examples)

No-relation (single object)

- color: Navigate to the {color} {object}.
- color-only: Navigate to the {color} object.
- no-color: Navigate to the {object}.

Relational (spatial grounding)

- ref: Navigate to the {color} {object} {rel} {refA}
- combined: Navigate to the {color} {object} {rel} {refA} and {rel} {refB}.

Example Prompts:

- Navigate to the green plant.
- Navigate to the green object.
- Navigate to the plant.
- Navigate to the green plant left of the chair.
- Navigate to the green plant left of the chair and right of the door.

Fig. 3: The left panels show two example indoor environments (Room A and Room B) with diverse furniture, objects, and layouts, illustrating the visual complexity encountered during training. The right panel summarizes the structured language prompt templates used for adapter training. Controlled linguistic variation and spatial relations encourage compositional understanding and support generalization to OOD objects, layouts, and relational configurations at evaluation time.

and spatial reasoning rather than memorization of object appearance or layout.

c) Privileged Expert: The privileged expert policy is trained with PPO using low-dimensional privileged state s_t as described in Section III. After convergence, the expert is frozen. We extract the expert latent z_t from a fixed internal layer (256-D) to supervise adapter training.

d) Adapter Training Data: To train the adapter, we roll out the expert in the training environment and record tuples (I_t, a_t) at each time step. Images are rendered from the agent’s onboard camera. Eight to nine different set of language instructions for each object are predefined and were sampled randomly during training. Only the adapter is trained; the expert and VLM are frozen.

e) Baselines: We compare LCLA against representative end-to-end methods and targeted ablations:

- Privileged Policy:** A PPO policy trained directly from privileged state observations to actions [34]. This policy is used to collect expert trajectories and serves as an upper bound for in-distribution performance (Room A).
- Language-Conditioned Behavior Cloning (LCBC):** This baseline removes latent alignment and directly predicts expert actions from visual–language observations. It uses the same backbone and encoder architecture as LCLA, but replaces the latent adapter and frozen action head with a trainable action predictor (an MLP mapping $256 \rightarrow 128 \rightarrow$ action), matching the structure of the expert action head. This controlled ablation isolates the effect of latent alignment by changing only the prediction target from latent representations to actions.
- Pooled-Embedding Latent Alignment (PELA):** PELA ablates explicit language conditioning within the adapter by aligning expert latents from pooled vision–language embeddings rather than token-level representations.

Specifically, we extract global image and text features from a frozen VLM using its image and text projection heads, and concatenate these pooled embeddings to form a joint representation. This joint embedding is then mapped to the expert latent via an MLP (embeddings $\rightarrow 512 \rightarrow 512 \rightarrow \hat{z}$). The perception backbone, expert latent target, and alignment objective are otherwise unchanged. This ablation isolates the effect of explicit language conditioning in the adapter, independent of the underlying vision–language representations.

• LeLaN: A language-conditioned navigation policy trained on large-scale augmented egocentric data using foundation models for supervision [13]. Although not fine-tuned on our environment, LeLaN benefits from navigation-specific vision–language supervision, whereas our approach uses off-the-shelf vision–language encoders, making the comparison conservative in favor of LeLaN.

f) Metrics.: We report **Success Rate** (SR) and **SPL** (Success weighted by Path Length). SR measures whether the goal is reached; SPL measures efficiency given the shortest path. All results are averaged over random seeds and episode initializations (30 episodes per goal).

g) Training details.: We collect 52k expert rollout steps by executing the frozen PPO policy in the training environment. To improve robustness under limited environment diversity, we augment the visual observations offline using aggressive appearance transformations. Specifically, for each original observation, we generate four additional augmented views using random combinations of cropping, color jitter, contrast and sharpness changes, blurring, perspective distortion, noise injection, and random erasing. This results in an effective training set of approximately 260k visual–language samples (one original and four augmented views per rollout

step). The adapter is then trained in a fully supervised manner for 10 epochs to align visual–language embeddings to the corresponding expert latent representations. All the results presented are with Siglip2 base model as backbone, unless stated.

V. RESULTS

We evaluate Language-Conditioned Latent Alignment (LCLA) and its controlled ablations in both the training environment (in-distribution, Room A) and an unseen evaluation environment (out-of-distribution, Room B). Performance is measured using Success Rate (SR), Success weighted by Path Length (SPL), and collision rate. Table II reports the primary quantitative results, while Tables III and IV present targeted ablations probing the structure and robustness of the latent interface.

a) Overall comparison.: The privileged PPO policy achieves near-perfect performance in Room A, confirming that the task is readily solvable when full state information is available. Among deployable agents, LCLA consistently outperforms both of its ablations (LCBC and PELA) as well as LeLaN across all metrics in both environments. This trend highlights the importance of simultaneously enforcing a task-centric latent interface and explicit language conditioning, rather than relying on direct action imitation or pooled representations.

b) In-distribution performance.: In Room A, LCLA achieves an SR of 90.4% and an SPL of 0.90, substantially outperforming its ablations LCBC (60.1% SR, 0.59 SPL) and PELA (62.5% SR, 0.62 SPL). While PELA improves modestly over LCBC by predicting expert latents rather than actions, the absence of language conditioning limits its effectiveness. LeLaN attains comparable performance to the ablations but remains far below LCLA. Although the privileged PPO policy remains superior due to access to full state information, LCLA significantly narrows the gap while remaining fully deployable. LCLA also exhibits markedly lower collision rates than all baselines, indicating more stable control even in the training environment.

c) Out-of-distribution generalization.: In the unseen Room B environment, LCLA maintains strong zero-shot performance with an SR of 80.5% and an SPL of 0.80. This represents a large absolute improvement over both LCBC (49.3% SR, 0.49 SPL) and PELA (57.6% SR, 0.58 SPL), demonstrating that latent alignment without language conditioning is insufficient under distribution shift. While LeLaN generalizes better than direct behavior cloning, it remains substantially less reliable than LCLA. Notably, LCLA reduces collision rates by more than 2 \times relative to all baselines, suggesting that explicit latent alignment improves both robustness and safety.

d) Latent interface dimensionality.: Table III evaluates LCLA using expert latent interfaces of varying dimensionality ($d_z \in \{128, 256, 512\}$). For each setting, a separate adapter is trained to predict the corresponding PPO hidden representation while reusing the matching frozen action head. Performance peaks sharply at $d_z = 256$, while both smaller and larger

latent dimensions lead to substantial degradation. This result indicates that effective alignment depends on the structure of the expert representation rather than its capacity.

e) Effect of vision–language backbone and robustness.

Table IV analyzes robustness to illumination and camera pose perturbations across different frozen vision–language backbones within the LCLA framework. Performance degrades systematically as the backbone weakens: CLIP exhibits strong sensitivity to lighting and viewpoint shifts, SigLIP shows partial robustness, and SigLIP2 maintains stable performance across all tested conditions. Crucially, these trends hold despite identical adapters and a frozen control policy, indicating that robustness under distribution shift is primarily inherited from the quality of the underlying visual representation.

VI. DISCUSSION

The results highlight a clear separation between task competence, perceptual generalization, and training regime. The privileged PPO expert achieves near-optimal performance when full state information is available, confirming that the navigation task is readily solvable given access to compact geometric variables. However, such policies are not deployable in realistic settings, motivating approaches that preserve expert control structure while operating from raw sensory inputs.

LCLA is not proposed as a full-stack navigation system or a benchmark for navigation performance. Accordingly, we do not compare against map-centric or topological approaches such as VLMaps [15], ZSON [24], or LM-Nav [36], which jointly address perception, mapping, memory, and planning. Instead, LCLA targets a narrower question: *can expert navigation behavior be recovered by aligning perception to a frozen, task-centric latent interface, without retraining control or constructing maps?* These paradigms are complementary rather than directly comparable.

Our ablations clarify the necessity of each component. LCBC removes latent alignment and directly predicts actions, resulting in brittle behavior under distribution shift, characterized by inefficient trajectories and high collision rates. PELA retains latent alignment but removes explicit language conditioning, yielding moderate improvements over LCBC but still substantial degradation relative to LCLA. These results indicate that neither end-to-end imitation nor latent alignment alone is sufficient; robust navigation requires aligning visual–language observations to the *correct* task-centric representation.

In contrast, LCLA consistently achieves strong performance across both in-distribution and out-of-distribution environments. By enforcing a fixed perception–control interface, LCLA preserves expert decision logic while confining perceptual uncertainty to a lightweight adapter. Robustness to lighting and viewpoint perturbations suggests reduced reliance on superficial visual statistics. Our language evaluation uses controlled, templated instructions to isolate perceptual grounding effects; extending to more naturalistic language remains an important direction for future work.

Model	In-Distribution (Room A)			Out-of-Distribution (Room B)			Efficiency	
	SR (%)	SPL	Coll. (%)	SR (%)	SPL	Coll. (%)	Params (M)	Inference time (ms)
Privileged PPO (Upper Bound)	97.7	0.977	2.3	–	–	–	0.49	5.00
LeLaN (General Model)	61.1	0.606	33.7	54.8	0.548	41.1	181.9	135.74
LCBC	60.1	0.591	39.7	49.3	0.491	45.0	13.7	75.41
PELA	62.5	0.616	37.5	57.6	0.576	40.9	1.2	69.06
LCLA	90.4	0.903	9.6	80.5	0.804	15.5	13.0	74.24

TABLE II: Task performance and computational efficiency across in-distribution (Room A) and out-of-distribution (Room B) environments. We report Success Rate (SR), Success weighted by Path Length (SPL), and collision rate, along with parameter count and per-step inference latency (RTX 4090, with IsaacSim running). We compare a privileged upper bound, language conditioned behavior cloning, pooled-embedding latent alignment, and language-conditioned latent alignment. LCLA achieves strong performance under distribution shift while remaining lightweight and significantly faster than large end-to-end vision-language policies. The privileged PPO policy is evaluated only in-distribution due to reliance on state information.

Latent Dimension (Room B)	d_z	SR (%)	SPL
Reduced latent	128	47.0	0.465
Default latent	256	80.5	0.804
Expanded latent	512	46.1	0.461

TABLE III: Effect of latent dimensionality on out-of-distribution performance. All rows correspond to the same LCLAA agent with different output latent dimensions. Matching the adapter output dimension to the expert latent space ($d_z = 256$) is critical for stable latent alignment; both smaller and larger dimensions lead to severe performance degradation.

Additional ablations reinforce this interpretation. Latent dimensionality experiments show that increasing representation capacity does not improve performance and can be detrimental, indicating that not all expert representations are equally suitable as control interfaces. Backbone comparisons further demonstrate that perception quality and control competence are separable: stronger visual representations improve alignment without modifying the control policy.

Several limitations remain. The privileged expert encodes obstacle information through simulator-derived geometry, and inferring equivalent abstractions from RGB alone may not scale to highly cluttered or real-world scenes. Our stability analyses are empirical rather than formal, and behavior under large alignment errors is not characterized. Finally, because the control policy is frozen, LCLA inherits the expert’s capabilities and cannot address tasks requiring exploration, memory, or long-horizon planning beyond the expert’s scope.

Overall, these findings suggest that robust generalization in embodied navigation can emerge from architectural constraints that enforce task-relevant information flow, rather than from larger models or end-to-end retraining.

VII. CONCLUSION

We introduced Language-Conditioned Latent Alignment (LCLA), a framework that reframes embodied navigation as a representation alignment problem rather than an end-to-end control learning problem. LCLA decouples perception from control by solving navigation once in a compact, task-centric

Backbone	Condition (Room B)	SR (%)	SPL
CLIP	Default OOD	62.5	0.625
	Very Low light	53.8	0.537
	Low light	63.9	0.638
	High light	59.6	0.596
	Very high light	61.3	0.613
	Lowered camera (-0.2 m)	56.4	0.564
SigLIP	Raised camera (+0.2 m)	57.4	0.572
	Default OOD	77.1	0.765
	Very Low light	64.6	0.643
	Low light	71.3	0.707
	High light	71.9	0.716
	Very high light	75.0	0.746
SigLIP2	Lowered camera (-0.2 m)	65.4	0.651
	Raised camera (+0.2 m)	72.4	0.720
	Default OOD	80.5	0.804
	Very Low light	70.9	0.7044
	Low light	78.5	0.7835
	High light	84.8	0.845

TABLE IV: Backbone-dependent robustness of LCLA to illumination and camera pose perturbations in Room B. While all backbones degrade under extreme conditions, stronger vision-language representations (SigLIP, SigLIP2) exhibit substantially improved robustness to viewpoint and lighting shifts. All of them are the base models. Also, please see Appendix for the lighting conditions and camera height. Figs 5 and 3.

latent space defined by a privileged expert and then learning to recover this representation from vision and language.

Through controlled ablations, we show that neither direct action imitation (LCBC) nor latent alignment without language conditioning (PELA) is sufficient to recover expert-level behavior under distribution shift. In contrast, LCLA consistently achieves higher success rates, more efficient trajectories, and lower collision rates across both in-distribution and out-of-distribution environments, without access to privileged information at test time.

Rather than proposing a new navigation policy, this work

advances a methodological claim: expert controllers can be reused across sensing modalities, perception backbones, and environments by enforcing a stable latent interface between perception and control. This perspective shifts the focus from learning policies from scratch toward identifying and recovering task-relevant representations that make control reliable.

Looking forward, future work will extend latent alignment to experts with memory and planning, richer and more naturalistic language grounding, and real-world robotic platforms, as well as develop stronger theoretical characterizations of latent suitability and alignment robustness.

VIII. ACKNOWLEDGMENT

This work is jointly funded from NSF-USDA COALESCE grant #2021-67021-34418 and NSF CNS-2313104.

REFERENCES

- [1] Rishabh Agarwal, Max Schwarzer, Pablo Samuel Castro, Aaron C Courville, and Marc Bellemare. Deep reinforcement learning at the edge of the statistical precipice. In M. Ranzato, A. Beygelzimer, Y. Dauphin, P.S. Liang, and J. Wortman Vaughan, editors, *Advances in Neural Information Processing Systems*, volume 34, pages 29304–29320. Curran Associates, Inc., 2021.
- [2] Dong An, Hanqing Wang, Wenguan Wang, Zun Wang, Yan Huang, Keji He, and Liang Wang. Etpnav: Evolving topological planning for vision-language navigation in continuous environments. *IEEE Transactions on Pattern Analysis and Machine Intelligence*, 47(7):5130–5145, 2025.
- [3] Peter Anderson, Qi Wu, Damien Teney, Jake Bruce, Mark Johnson, Niko Sünderhauf, Ian Reid, Stephen Gould, and Anton van den Hengel. Vision-and-language navigation: Interpreting visually-grounded navigation instructions in real environments. In *Proceedings of the IEEE Conference on Computer Vision and Pattern Recognition (CVPR)*, June 2018.
- [4] Elliot Chane-Sane, Joseph Amigo, Thomas Flayols, Ludovic Righetti, and Nicolas Mansard. Soloparkour: Constrained reinforcement learning for visual locomotion from privileged experience, 2024.
- [5] Devendra Singh Chaplot, Ruslan Salakhutdinov, Abhinav Gupta, and Saurabh Gupta. Neural topological slam for visual navigation. In *Proceedings of the IEEE/CVF Conference on Computer Vision and Pattern Recognition (CVPR)*, June 2020.
- [6] Dian Chen, Brady Zhou, Vladlen Koltun, and Philipp Krähenbühl. Learning by cheating. In Leslie Pack Kaelbling, Danica Kragic, and Komei Sugiura, editors, *Proceedings of the Conference on Robot Learning*, volume 100 of *Proceedings of Machine Learning Research*, pages 66–75. PMLR, 30 Oct–01 Nov 2020.
- [7] Vishnu Sashank Dorbala, Gunnar Sigurdsson, Robinson Piramuthu, Jesse Thomason, and Gaurav S. Sukhatme. Clip-nav: Using clip for zero-shot vision-and-language navigation, 2022.
- [8] Daniel Fried, Ronghang Hu, Volkan Cirik, Anna Rohrbach, Jacob Andreas, Louis-Philippe Morency, Taylor Berg-Kirkpatrick, Kate Saenko, Dan Klein, and Trevor Darrell. Speaker-follower models for vision-and-language navigation. In S. Bengio, H. Wallach, H. Larochelle, K. Grauman, N. Cesa-Bianchi, and R. Garnett, editors, *Advances in Neural Information Processing Systems*, volume 31. Curran Associates, Inc., 2018.
- [9] Robert Geirhos, Jörn-Henrik Jacobsen, Claudio Michaelis, Richard Zemel, Wieland Brendel, Matthias Bethge, and Felix A. Wichmann. Shortcut learning in deep neural networks. *Nature Machine Intelligence*, 2(11):665–673, November 2020.
- [10] Saurabh Gupta, James Davidson, Sergey Levine, Rahul Sukthankar, and Jitendra Malik. Cognitive mapping and planning for visual navigation. In *Proceedings of the IEEE Conference on Computer Vision and Pattern Recognition (CVPR)*, July 2017.
- [11] David Ha and Jürgen Schmidhuber. Recurrent world models facilitate policy evolution. In S. Bengio, H. Wallach, H. Larochelle, K. Grauman, N. Cesa-Bianchi, and R. Garnett, editors, *Advances in Neural Information Processing Systems*, volume 31. Curran Associates, Inc., 2018.
- [12] Danijar Hafner, Timothy Lillicrap, Jimmy Ba, and Mohammad Norouzi. Dream to control: Learning behaviors by latent imagination, 2020.
- [13] Noriaki Hirose, Catherine Glossop, Ajay Sridhar, Dhruv Shah, Oier Mees, and Sergey Levine. Lelan: Learning a language-conditioned navigation policy from in-the-wild videos, 2024.
- [14] Haodong Hong, Yanyuan Qiao, Sen Wang, Jiajun Liu, and Qi Wu. General scene adaptation for vision-and-language navigation, 2025.
- [15] Chenguang Huang, Oier Mees, Andy Zeng, and Wolfram Burgard. Visual language maps for robot navigation, 2023.
- [16] Seongjun Jeong, Gi-Cheon Kang, Seongho Choi, Joochan Kim, and Byoung-Tak Zhang. Continual vision-and-language navigation, 2025.
- [17] Jens Kober, J. Andrew Bagnell, and Jan Peters. Reinforcement learning in robotics: A survey. *The International Journal of Robotics Research*, 32(11):1238–1274, 2013.
- [18] Jacob Krantz, Erik Wijmans, Arjun Majumdar, Dhruv Batra, and Stefan Lee. Beyond the nav-graph: Vision-and-language navigation in continuous environments. In Andrea Vedaldi, Horst Bischof, Thomas Brox, and Jan-Michael Frahm, editors, *Computer Vision – ECCV 2020*, pages 104–120, Cham, 2020. Springer International Publishing.
- [19] Michael Laskin, Aravind Srinivas, and Pieter Abbeel. CURL: Contrastive unsupervised representations for reinforcement learning. In Hal Daumé III and Aarti Singh, editors, *Proceedings of the 37th International Conference*

on Machine Learning, volume 119 of *Proceedings of Machine Learning Research*, pages 5639–5650. PMLR, 13–18 Jul 2020.

[20] Timothée Lessort, Natalia Díaz-Rodríguez, Jean-François Goudou, and David Filliat. State representation learning for control: An overview. *Neural Networks*, 108:379–392, December 2018.

[21] Sergey Levine, Chelsea Finn, Trevor Darrell, and Pieter Abbeel. End-to-end training of deep visuomotor policies, 2016.

[22] Qixiu Li, Yu Deng, Yaobo Liang, Lin Luo, Lei Zhou, Chengtang Yao, Lingqi Zeng, Zhiyuan Feng, Huizhi Liang, Sicheng Xu, Yizhong Zhang, Xi Chen, Hao Chen, Lily Sun, Dong Chen, Jiaolong Yang, and Baining Guo. Scalable vision-language-action model pretraining for robotic manipulation with real-life human activity videos, 2025.

[23] Yidan Lu, Rurui Yang, Qiran Kou, Mengting Chen, Tao Fan, Peter Cui, Yinzhaodong, and Peng Lu. Contrastive representation learning for robust sim-to-real transfer of adaptive humanoid locomotion, 2025.

[24] Arjun Majumdar, Gunjan Aggarwal, Bhavika Suresh Devnani, Judy Hoffman, and Dhruv Batra. ZSON: Zero-shot object-goal navigation using multimodal goal embeddings. In Alice H. Oh, Alekh Agarwal, Danielle Belgrave, and Kyunghyun Cho, editors, *Advances in Neural Information Processing Systems*, 2022.

[25] Nico Messikommer, Jiaxu Xing, Elie Aljalbout, and Davide Scaramuzza. Student-informed teacher training, 2025.

[26] Piotr Mirowski, Razvan Pascanu, Fabio Viola, Hubert Soyer, Andrew J. Ballard, Andrea Banino, Misha Denil, Ross Goroshin, Laurent Sifre, Koray Kavukcuoglu, Dharshan Kumaran, and Raia Hadsell. Learning to navigate in complex environments, 2017.

[27] Gianluca Monaci, Michel Aractingi, and Tomi Silander. DiPCAN: Distilling Privileged Information for Crowd-Aware Navigation. In *Proceedings of Robotics: Science and Systems*, New York City, NY, USA, June 2022.

[28] Amr Mousa, Neil Karavis, Michele Caprio, Wei Pan, and Richard Allmendinger. Tar: Teacher-aligned representations via contrastive learning for quadrupedal locomotion, 2025.

[29] Lerrel Pinto, Marcin Andrychowicz, Peter Welinder, Wojciech Zaremba, and Pieter Abbeel. Asymmetric actor critic for image-based robot learning, 2017.

[30] Alec Radford, Jong Wook Kim, Chris Hallacy, Aditya Ramesh, Gabriel Goh, Sandhini Agarwal, Girish Sastry, Amanda Askell, Pamela Mishkin, Jack Clark, Gretchen Krueger, and Ilya Sutskever. Learning transferable visual models from natural language supervision. In Marina Meila and Tong Zhang, editors, *Proceedings of the 38th International Conference on Machine Learning*, volume 139 of *Proceedings of Machine Learning Research*, pages 8748–8763. PMLR, 18–24 Jul 2021.

[31] Aravind Rajeswaran, Sarvjeet Ghora, Balaraman Ravinder, and Sergey Levine. Epopt: Learning robust neural network policies using model ensembles, 2017.

[32] Andrei A. Rusu, Matej Večerík, Thomas Rothörl, Nicolas Heess, Razvan Pascanu, and Raia Hadsell. Sim-to-real robot learning from pixels with progressive nets. In Sergey Levine, Vincent Vanhoucke, and Ken Goldberg, editors, *Proceedings of the 1st Annual Conference on Robot Learning*, volume 78 of *Proceedings of Machine Learning Research*, pages 262–270. PMLR, 13–15 Nov 2017.

[33] Manolis Savva, Abhishek Kadian, Oleksandr Maksymets, Yili Zhao, Erik Wijmans, Bhavana Jain, Julian Straub, Jia Liu, Vladlen Koltun, Jitendra Malik, Devi Parikh, and Dhruv Batra. Habitat: A platform for embodied ai research. In *2019 IEEE/CVF International Conference on Computer Vision (ICCV)*, pages 9338–9346, 2019.

[34] John Schulman, Filip Wolski, Prafulla Dhariwal, Alec Radford, and Oleg Klimov. Proximal policy optimization algorithms, 2017.

[35] Pierre Sermanet, Corey Lynch, Yevgen Chebotar, Jasmine Hsu, Eric Jang, Stefan Schaal, Sergey Levine, and Google Brain. Time-contrastive networks: Self-supervised learning from video. In *2018 IEEE International Conference on Robotics and Automation (ICRA)*, pages 1134–1141, 2018.

[36] Dhruv Shah, Blazej Osinski, Brian Ichter, and Sergey Levine. Lm-nav: Robotic navigation with large pre-trained models of language, vision, and action, 2022.

[37] Michael Tschannen, Alexey Gritsenko, Xiao Wang, Muhammad Ferjad Naeem, Ibrahim Alabdulmohsin, Nikhil Parthasarathy, Talfan Evans, Lucas Beyer, Ye Xia, Basil Mustafa, Olivier Hénaff, Jeremiah Harmsen, Andreas Steiner, and Xiaohua Zhai. Siglip 2: Multilingual vision-language encoders with improved semantic understanding, localization, and dense features, 2025.

[38] Denis Yarats, Ilya Kostrikov, and Rob Fergus. Image augmentation is all you need: Regularizing deep reinforcement learning from pixels. In *International Conference on Learning Representations*, 2021.

[39] Xiaohua Zhai, Basil Mustafa, Alexander Kolesnikov, and Lucas Beyer. Sigmoid loss for language image pre-training. In *Proceedings of the IEEE/CVF International Conference on Computer Vision (ICCV)*, pages 11975–11986, October 2023.

[40] Amy Zhang, Rowan McAllister, Roberto Calandra, Yarin Gal, and Sergey Levine. Learning invariant representations for reinforcement learning without reconstruction, 2021.

[41] Linrui Zhang, Zhenghao Peng, Quanyi Li, and Bolei Zhou. Cat: Closed-loop adversarial training for safe end-to-end driving. In Jie Tan, Marc Toussaint, and Kourosh Darvish, editors, *Proceedings of The 7th Conference on Robot Learning*, volume 229 of *Proceedings of Machine Learning Research*, pages 2357–2372. PMLR, 06–09 Nov 2023.

[42] Duo Zheng, Shijia Huang, Yanyang Li, and Liwei Wang.

Efficient-VLN: A training-efficient vision-language navigation model, 2025.

- [43] Yuke Zhu, Roozbeh Mottaghi, Eric Kolve, Joseph J. Lim, Abhinav Gupta, Li Fei-Fei, and Ali Farhadi. Target-driven visual navigation in indoor scenes using deep reinforcement learning. In *2017 IEEE International Conference on Robotics and Automation (ICRA)*, pages 3357–3364, 2017.

APPENDIX

This appendix summarizes the configuration used to train the *privileged PPO teacher* in Isaac Lab for the Jetbot navigation task. We report the environment design choices, observation/action spaces, domain randomization parameters, reward shaping terms, and termination conditions. (Implementation-specific function and file names are omitted.)

A. Environment and Simulation Settings

a) *Vectorized simulation*.: Training uses $N_{\text{env}} = 16$ parallel environments with environment spacing of 50 units and replicated physics enabled. The control decimation is 2, with a simulation step of $\Delta t = 1/60$ s, yielding an effective control step of 2/60 s. Episodes are capped at 15 s.

b) *Physics and rendering*.: The simulation uses GPU dynamics with a TGS solver and GPU broadphase. Rendering is configured in performance mode with RTX features enabled (global illumination, reflections, shadows, denoisers), using 1 sample per pixel. Ambient light intensity is set to zero. A dome HDR environment light is used (HDRI texture, intensity 1000).

c) *Robot actuation*.: The robot is controlled as a differential-drive system via direct wheel *velocity targets*. The action scale is 40.0 (rad/s). Actuator configuration uses velocity limits of 20.0 (rad/s), zero stiffness, and damping 10.0, emphasizing velocity-control dynamics over position-control behavior.

B. Goal Set and Reset Strategy

a) *Goal set*.: A discrete set of semantic goals is defined (e.g., door, desk, TV, chairs, plants, lamp, trash can, etc.). Each goal may have one or more candidate (x, y) target coordinates. On reset, a goal is sampled uniformly and a specific variant is selected (closest variant to the start pose when multiple are available).

b) *Room bounds and safe goal adjustment*.: The navigable region is bounded by a fixed axis-aligned box:

$$(x_{\min}, y_{\min}, x_{\max}, y_{\max}) = (-4.25, -3.64, 6.5, 3.5).$$

A “safe” goal position is computed by moving the goal slightly toward the room center by a configurable clearance and then clamping to the room bounds with a small margin, preventing targets from landing outside valid space or too close to edges.

c) *Start pose*.: The robot resets to a fixed start position (shared across environments), and the yaw is set to face the current goal with added uniform noise of ± 0.5 radians (approximately $\pm 28.6^\circ$), improving robustness to initial heading perturbations.

C. Observation Space

a) *Privileged PPO observation*.: The PPO teacher uses a privileged state vector of dimension 159, composed of:

- **Base navigation state** (9 dims):

$$[g_x, g_y, \sin(\beta), \cos(\beta), v_x, v_y, \omega, \dot{q}_L, \dot{q}_R],$$

where (g_x, g_y) is the goal position in the robot body frame, β is the bearing angle to the goal, (v_x, v_y) is planar

velocity in body frame, ω is yaw rate, and (\dot{q}_L, \dot{q}_R) are left/right wheel velocities.

- **Obstacle features** (150 dims): $K = 50$ obstacle clusters, each represented by three body-frame quantities

$$[o_x, o_y, d] \in \mathbb{R}^3,$$

normalized by a maximum obstacle distance $d_{\max} = 5.0$ m. Total obstacle feature dimensionality is $50 \times 3 = 150$.

b) *Obstacle clustering*.: Obstacle centers are extracted from a 2D occupancy map generated on the USD stage (cell size 0.05 m) within fixed bounds. Occupied cells are clustered into $K = 50$ centroids via k -means, yielding a compact, fixed-size obstacle representation.

c) *Normalization*.: Obstacle coordinates and distances are normalized by d_{\max} before concatenation. Goal coordinates are represented in the robot body frame, and bearing is encoded with sin / cos to avoid angle discontinuities.

d) *Optional sensory logging*.: RGB and depth camera outputs (single tiled camera) are captured for evaluation/logging and stored as auxiliary outputs; they are not used as privileged PPO observations in this configuration.

D. Action Space and Control

The action space is continuous with dimension 2:

$$a = [a_L, a_R] \in [-1, 1]^2,$$

scaled by $s_a = 40.0$ to produce wheel velocity targets in rad/s:

$$\dot{q}^* = s_a \cdot a.$$

These targets are applied directly to the wheel joints each control step.

E. Domain Randomization

Domain randomization is applied *on reset* via event terms.

a) *Material randomization*.: A set of apartment object prim paths (furniture, electronics, decorations, small objects, structural elements, and door) are randomized by:

- sampling a diffuse display color uniformly from a default RGB range $[0.1, 0.9]^3$,
- unbinding existing materials on mesh children so the display color is visible,
- (optionally) randomizing roughness in $[0.2, 0.8]$ and metallic in $[0.0, 0.3]$.

To preserve task semantics, objects corresponding to the *currently selected goal* are excluded from material randomization in each environment.

b) *Lighting randomization (optional)*.: Support is included to randomize directional light intensity, angle, and orientation, as well as renderer auto-exposure settings. In the provided configuration, an HDR dome light is active; directional-light randomization can be enabled similarly when used.

F. Reward Function

The reward is a sum of shaped components designed to provide dense learning signal while enforcing safety:

a) (1) *Progress and potential-based shaping*.: Let d_t be current distance to goal and d_{t-1} the previous distance. Progress reward:

$$r_{\text{prog}} = (d_{t-1} - d_t), \quad \lambda_{\text{prog}} = 15.0.$$

A distance potential term provides a smooth shaping signal:

$$r_{\text{pot}} = -\lambda_{\text{pot}} \left(1 - e^{-d_t/5}\right) \cdot 5, \quad \lambda_{\text{pot}} = 2.0.$$

b) (2) *Heading alignment*.: Let \hat{h} be the unit heading direction and \hat{g} be the unit direction to the goal. The facing reward uses exponential shaping:

$$r_{\text{face}} = \lambda_{\text{face}} \left(e^{\langle \hat{h}, \hat{g} \rangle} - 1\right), \quad \lambda_{\text{face}} = 5.0.$$

c) (3) *Forward motion when aligned*.: Forward motion is rewarded only when the robot is oriented toward the goal ($\langle \hat{h}, \hat{g} \rangle > 0$):

$$r_{\text{fwd}} = \lambda_{\text{fwd}} \|\mathbf{v}_{xy}\| \max(0, \langle \hat{h}, \hat{g} \rangle), \quad \lambda_{\text{fwd}} = 0.5.$$

d) (4) *Obstacle avoidance penalty*.: Obstacle distances are computed in world coordinates from clustered centers. Obstacles near the goal (within 1.5 m) and obstacles extremely close to the robot (within 0.3 m) are excluded from penalty computation. Let d_{min} be the minimum remaining obstacle distance, and $d_{\text{th}} = 0.5$ m. The penalty is:

$$r_{\text{obs}} = \lambda_{\text{obs}} \cdot \text{clip}\left(\frac{d_{\text{th}} - d_{\text{min}}}{d_{\text{th}}}, 0, 1\right), \quad \lambda_{\text{obs}} = -3.0.$$

e) (5) *Boundary penalty*.: If the robot leaves the room bounds, a fixed penalty is applied:

$$r_{\text{bnd}} = \lambda_{\text{bnd}} \cdot \mathbb{I}[\text{out of bounds}], \quad \lambda_{\text{bnd}} = -10.0.$$

f) (6) *Success bonus*.: Success is declared when distance and heading are within thresholds:

$$d_t < d_{\text{succ}} = 1.5 \text{ m}, \quad |\theta_{\text{err}}| < \theta_{\text{succ}} = \pi/6.$$

A large terminal bonus is added:

$$r_{\text{succ}} = \lambda_{\text{succ}} \cdot \mathbb{I}[\text{success}], \quad \lambda_{\text{succ}} = 200.0.$$

g) *Total reward*.: The final reward is:

$$r_t = \lambda_{\text{prog}} r_{\text{prog}} + r_{\text{pot}} + r_{\text{face}} + r_{\text{fwd}} + r_{\text{obs}} + r_{\text{bnd}} + r_{\text{succ}}.$$

G. Termination and Truncation

Episodes terminate upon:

- **Success**: meeting the distance and angle thresholds above.
- **Hard collision**: when the maximum contact force magnitude exceeds a small threshold (10^{-5} as configured).
- **Timeout**: reaching the episode length limit (15 s).

Timeout is treated as truncation only when neither success nor collision has occurred.

H. Sensors and Auxiliary Signals

A contact sensor is enabled on the robot to measure net forces used for collision termination. A forward-facing RGB camera is instantiated for evaluation-time logging.

This appendix provides implementation details, training objectives, and robustness analyses omitted from the main text for clarity. These details support the Language-Conditioned Latent Alignment Adapter (LCLAA), which serves as a concrete instantiation of the broader **LCLAA** framework. Our goal here is to document architectural and training choices rather than introduce additional contributions.

I. Architectural Details of LCLAA

a) *Patch Projection and Contextualization*.: Given patch-level visual embeddings $V_t \in \mathbb{R}^{N \times D_{\text{img}}}$ from a frozen vision-language model, LCLAA first projects them into a shared hidden space of dimension H :

$$X_t^0 = V_t W_p + \mathbf{1} b_p^\top.$$

To incorporate spatial context and interactions between patches, we apply multi-head self-attention (MHSA) with residual connections and layer normalization:

$$X_t = \text{LayerNorm}(X_t^0 + \text{MHSA}(X_t^0)).$$

This step allows local visual features to integrate global scene information prior to instruction conditioning.

b) *Language-Conditioned Spatial Attention*.: To identify instruction-relevant visual regions, each contextualized patch embedding $x_{t,i}$ is scored conditioned on the language embedding T :

$$\tilde{T} = TW_s + b_s, \quad s_{t,i} = g_\theta([x_{t,i}; \tilde{T}]),$$

where g_θ is a lightweight multilayer perceptron. The scores are normalized using a temperature-scaled softmax:

$$\alpha_{t,i} = \frac{\exp(s_{t,i}/\tau)}{\sum_{j=1}^N \exp(s_{t,j}/\tau)}.$$

During training, we optionally inject Gumbel noise into $s_{t,i}$ prior to normalization to encourage stochastic exploration of patch relevance while retaining differentiability.

c) *Differentiable Bottleneck via Visual Aggregation*.: Rather than forwarding all patch embeddings downstream, LCLAA enforces a strict information bottleneck by aggregating visual features into a single token:

$$\bar{x}_t = \sum_{i=1}^N \alpha_{t,i} x_{t,i}.$$

This operation forms a convex combination of contextualized patch embeddings, ensuring that downstream control has access only to a compact, instruction-conditioned summary of the scene.

d) Query Construction and Cross-Attention Refinement.:

To refine the bottleneck representation, LCLAA constructs a set of query tokens consisting of a text-derived query and a small number of learnable queries:

$$q_t^{(0)} = TW_q + b_q, \quad Q_t^0 = [q_t^{(0)}; q^{(1)}; \dots; q^{(M)}].$$

Keys and values are derived from the bottleneck token \bar{x}_t . The queries are refined using a stack of B cross-attention blocks (CABs), each composed of multi-head cross-attention followed by a feed-forward network with residual connections:

$$Q_t^{(b+1)} = \text{CAB}_\theta(Q_t^{(b)}, K_t, V_t), \quad b = 0, \dots, B - 1.$$

e) Gated Fusion and Latent Projection.: The refined query tokens are flattened and fused with the language embedding using a learned gating mechanism:

$$h_t = g_t \odot \tilde{h}_t + (1 - g_t) \odot t_t,$$

where $g_t \in (0, 1)^H$ is a sigmoid gate, \tilde{h}_t is a linear projection of the concatenated queries, and t_t is the projected text embedding. The fused representation is then mapped to the expert latent space using a multilayer perceptron:

$$\hat{z}_t = \text{MLP}_\theta(h_t).$$

J. Training Objectives

a) Latent Regression and Action Consistency.: Let z_t denote the latent representation produced by the privileged expert encoder at timestep t . LCLAA is trained using a supervised latent alignment objective that combines latent regression, contrastive alignment, and action consistency:

$$\mathcal{L} = \lambda_1 \mathcal{L}_{\text{contrast}} + (1 - \lambda_1) \|\hat{z}_t - z_t\|_2^2 + \lambda_2 \|\pi_{\text{priv}}^a(\hat{z}_t) - \pi_{\text{priv}}^a(z_t)\|_2^2, \quad (11)$$

where $\pi_{\text{priv}}^a(\cdot)$ denotes the action logits of the frozen expert policy.

b) Contrastive Latent Alignment.: We employ a symmetric InfoNCE loss to encourage discriminative and consistent alignment between predicted latents \hat{z} and expert latents z . For a minibatch of size B , the loss is defined as:

$$\mathcal{L}_{\text{InfoNCE}} = -\frac{1}{B} \sum_{i=1}^B \log \frac{\exp(\text{sim}(\hat{z}_i, z_i)/\tau)}{\sum_{j=1}^B \exp(\text{sim}(\hat{z}_i, z_j)/\tau)}.$$

The loss is applied symmetrically in both directions. We fix the temperature τ throughout training and do not ablate individual loss components, as our objective is to evaluate latent alignment as a representation learning paradigm rather than optimize loss design.

K. Latent Robustness and Action-Space Stability

a) Sensitivity of the Frozen Action Head.: A potential concern with freezing the action head is that imperfect latent alignment may produce representations that lie outside the distribution encountered during expert training. To assess this risk, we empirically estimate the Lipschitz constant L of the frozen action head π_{priv}^a , defined such that

$$\|\pi_{\text{priv}}^a(z_1) - \pi_{\text{priv}}^a(z_2)\| \leq L \|z_1 - z_2\|.$$

Across multiple trained experts, we observe an average empirical Lipschitz constant of $L \approx 0.16$, indicating smooth behavior in the neighborhood of the expert latent manifold.

b) Noise Injection Experiments.: We further evaluate robustness by injecting isotropic Gaussian noise into expert latents during deployment. Performance degrades gradually rather than catastrophically under increasing perturbations. With noise standard deviation $\sigma = 1.0$, the policy achieves a success rate of 100%; at $\sigma = 2.0$, success remains at 88%; and at $\sigma = 3.0$, the agent succeeds in 75.5% of episodes. These results indicate that bounded latent misalignment induces predictable and stable deviations in action space.

c) Discussion.: Together, the low empirical Lipschitz constant and graceful degradation under noise injection suggest that freezing the action head is a reasonable and stable design choice when the expert latent space is well-structured. While this does not constitute a formal robustness or safety guarantee, it provides empirical evidence that latent alignment errors do not lead to abrupt or unsafe failures in our setting.



Very High High Default Low Very Low

Fig. 4: Illumination intensity perturbations in the out-of-distribution Room B environment. Egocentric RGB observations are shown under very high, high, default, low, and very low lighting conditions. These controlled changes in global illumination significantly alter scene appearance, contrast, and shadowing, and are used to evaluate robustness to lighting variation.



-0.2 m Default +0.2 m

Fig. 5: Camera height perturbations in the out-of-distribution Room B environment. The agent's egocentric RGB observations are shown for a lowered camera (-0.2 m), the default camera height, and a raised camera ($+0.2\text{ m}$). These perturbations induce significant changes in visible floor area, object scale, and perspective, serving as a controlled test of viewpoint robustness.